ELSEVIER

Journal of Structural Geology 28 (2006) 170–183

JOURNAL OF STRUCTURAL GEOLOGY

www.elsevier.com/locate/jsg

Trishear kinematic modeling of extensional fault-propagation folding

Guohai Jin *, Richard H. Groshong Jr.

Department of Geological Sciences, The University of Alabama, Tuscaloosa, AL 35487, USA

Received 2 December 2003; received in revised form 20 January 2005; accepted 7 September 2005
Available online 7 November 2005

Abstract

We present a new non-linear 2-D numerical trishear model that is capable of modeling both symmetrical and asymmetrical trishear zones and a strain prediction approach based on the velocity field within the trishear zone. A simple relationship exists between the shape factor (r) of the velocity field, the hanging wall apical angle, and footwall apical angle. The implication of this relationship is that when dealing with a real deformed state cross-section, one can measure the hanging wall and footwall apical angles to determine the r value to specify the velocity field within the trishear zone for either the forward modeling or restoration. The new trishear model can accurately reproduce the geometry of two experimental clay models and an extensional fault-propagation fold from the Gulf of Suez. Predicted strain is greatest directly above the fault tip and decreases with distance from the fault tip, as in the experimental models. Greater strain occurs in the hanging wall because of the greater velocity gradient there, whereas the footwall is much less intensely deformed. Consequently, secondary faulting and fracturing, if present, should be better developed along the fault tip line or in the hanging wall. The orientation of fractures or minor faults can be predicted from the strain ellipses calculated from the trishear velocity field.

Keywords: Trishear; Kinematic modeling; Fault-propagation folding; Deformation

1. Introduction

Extensional fault-propagation folds commonly form as a result of the upward propagation of faults into regions that have been monoclinally flexed at the fault tips. Where the rate of fault propagation is slow with respect to the rate of fault displacement, a monocline will occur above the fault tip (Ferrill et al., 2004). Evidence from well-exposed folds with preserved growth strata (Gawthorpe et al., 1997), well based 3-D subsurface mapping (Jin et al., 1998), and from analog models (Withjack et al., 1990) and numerical models (Patton and Fletcher, 1995; Hardy and McClay, 1999) indicates that extensional fault-propagation folds form as upward widening monoclinal zones of distributed deformation above discrete faults at depth (Fig. 1). Extensional fault-propagation folds have been recognized from many areas of the world, e.g. the Rhine Graben (Laubscher, 1982), the North Sea (Withjack et al., 1989), the Gulf of Suez (Gawthorpe et al., 1997), and the Gulf of Mexico basin (Pashin et al., 2000). Due to the frequent occurrence of hydrocarbons associated with them and in the underlying fault blocks, extensional fault-propagation folds are receiving increasing attention in academic and industrial domains. While the geometry of extensional fault-propagation folds is reasonably well understood (Schlische, 1995; Janecke et al., 1998), the kinematic linkage between deeper faulting and shallower distributed deformation is a subject for further exploration.

The trishear kinematic model was first proposed by Erslev (1991) and Erslev and Rogers (1993). It was designed to predict the geometry of fault-propagation folds, which grow with changes both in bed thickness and dip on the fold limbs. Trishear is the distributed shear in a triangular zone, one apex of which is located at the tip of a fault. Hardy and Ford (1997) expanded Erslev's (1991) initial trishear model by presenting a clear mathematical formulation of the problem. They analyzed the effect of variable propagation to slip ratios and illustrated growth strata geometries associated with trishear fault-propagation folds in compressional geological settings. Allmendinger (1998) used Hardy and Ford's (1997) numerical trishear

* Corresponding author. Present address: Geological Survey of Alabama, P.O. Box 869999, Tuscaloosa, AL 35486, USA. Tel.: +1 205 2473560; fax: +1 205 2473560.
E-mail address: gjin@gsa.state.al.us (G. Jin).

0191-8141/$ - see front matter © 2005 Elsevier Ltd. All rights reserved.
doi:10.1016/j.jsg.2005.09.003

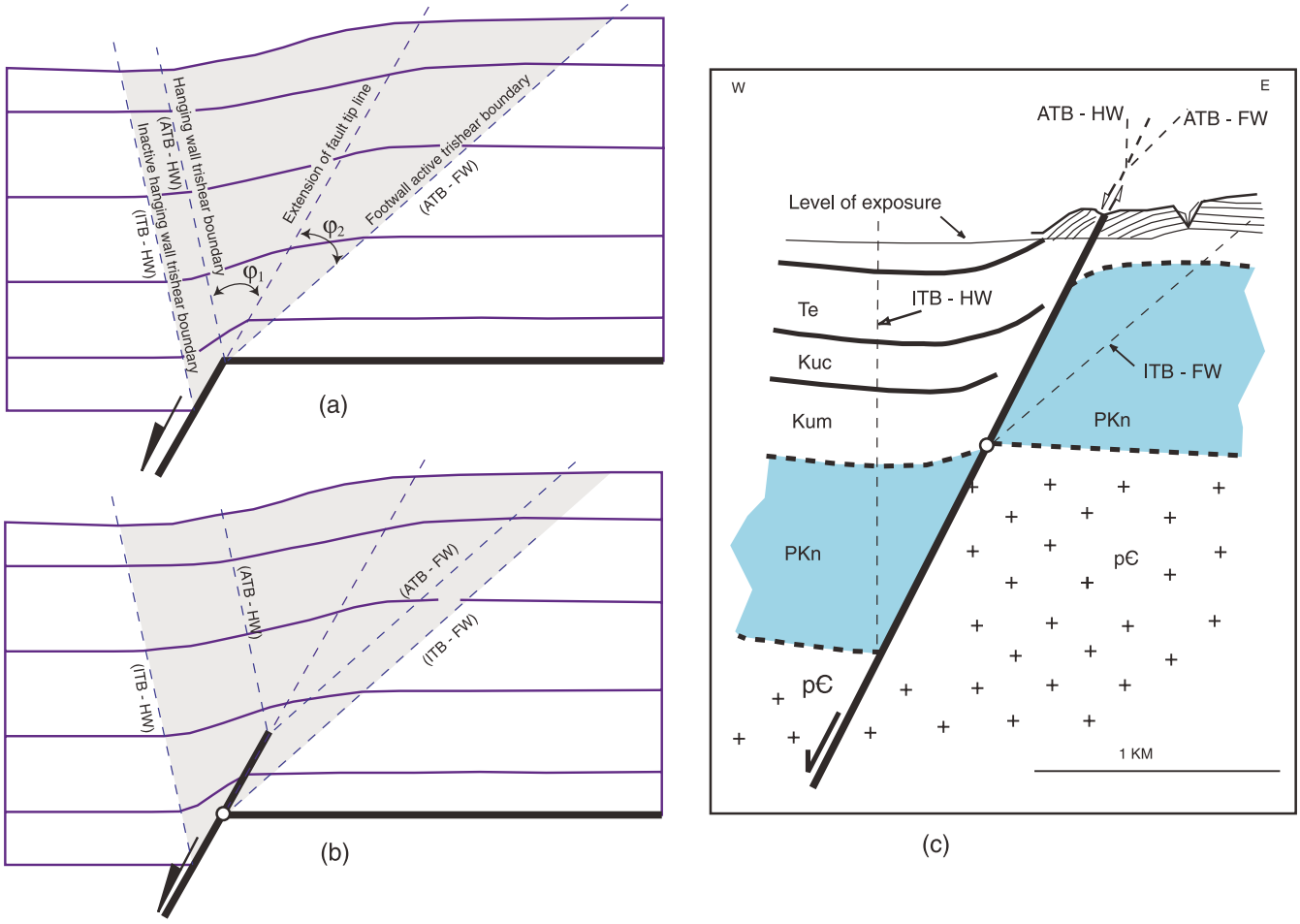

Fig. 1. Extensional fault-propagation folds associated with slip along the underlying faults. (a) Schematic diagram illustrating basic features of an extensional fold with a non-migrating fault tip. (b) Schematic diagram of an extensional fault-propagation fold. (c) Cross-section of extensional fault-propagation fold from the Gulf of Suez (modified from Withjack et al., 1990). No vertical exaggeration. Details of bed geometry are shown where observed in outcrop. pC = Precambian basement, PKn = Nubia sandstone, Kum = interbedded upper Cretaceous limestone and shale, Kuc = Paleocene and upper Cretaceous shale and limestone, Te = Eocene limestone. The shaded zone in (a) is the trishear deformation zone. ϕ_1 = hanging wall apical angle, ϕ_2 = footwall apical angle, HW = hanging wall, FW = footwall, ITB = inactive trishear boundary, ATB = active trishear boundary. Note that the open circles in (b) and (c) represent the location of the initial fault tip.

model to further discuss the influence of variable trishear parameters on the geometry of fault-propagation folds both in growth and pre-growth strata. Hardy and McClay (1999) applied the model to an experimental clay model made by Withjack et al. (1990) and concluded that the trishear model could accurately reproduce the geometry of extensional fault-propagation folds. Recently, Zehnder and Allmendinger (2000) proposed several velocity field models for a trishear zone and suggested that the velocity field could be expressed in a non-linear pattern.

In Erslev's (1991) original model, the trishear zone was fixed with respect to either the hanging wall or footwall of a fault, which is called a hanging wall fixed or footwall fixed trishear zone (Hardy and Ford, 1997). In this paper, we use additional terms to further describe the geometric features of extensional fault-propagation folds. The upward widening deformation zone of an extensional fault-propagation fold is defined by a hanging wall trishear boundary and a footwall trishear boundary, both of which are attached to the underlying fault tip. Within these two boundaries is an area where non-uniformly distributed shear deformation occurs that is called the trishear zone (Fig. 1a). The hanging wall trishear boundary and the footwall trishear boundary attached to the currently active fault tip are called the hanging wall active trishear boundary (ATB–HW) and footwall active trishear boundary (ATB–FW), respectively (Fig. 1a). As the displacement along the underlying fault increases, material points within the hanging wall trishear zone move continuously across the active trishear boundary. The boundary between deformed and undeformed parts of the hanging wall (Fig. 1a) is called the hanging wall inactive trishear boundary (ITB–HW). If the fault tip does not propagate during deformation, which is the case of footwall-attached trishear (Fig. 1a), the footwall active trishear boundary remains stationary and coincides with the initial footwall trishear boundary, called the footwall inactive

trishear boundary (ITB–FW). If, however, the fault propagates during the deformation, the footwall active trishear boundary will migrate upward along with the fault tip and become separate from the ITB–FW (Fig. 1b and c).

Although the numerical trishear model has been successful in modeling non-kink-band-style deformation (Allmendinger, 1998; Hardy and McClay, 1999), there are still problems with this model. First, experimental models (Withjack et al., 1990) and natural examples (Withjack et al., 1989; Hardy and McClay, 1999) suggest that the upward widening deformed zone (the trishear zone) is usually not symmetrical across the tip line of the underlying fault (Fig. 1, $\phi_1 \neq \phi_2$). This contradicts the predicted results from the numerical trishear model by Hardy and Ford (1997) using a linear velocity field method. It is evident that the linear velocity field model is not sufficient to properly predict or describe the general trishear deformation. Therefore, a more general form of trishear velocity needs to be formulated, and there is no need to limit those models to linear velocity field. The piece-wise linear trishear model proposed by Zehnder and Allmendinger (2000) avoids the symmetry problem, but their predicted trishear folds have a sharp kink-band like geometry within the trishear zone along the tip line of the underlying fault (Fig. 2a). The non-linear velocity field derived by Zehnder and Allmendinger (2000) is still limited to symmetrical trishear geometry (Fig. 2b).

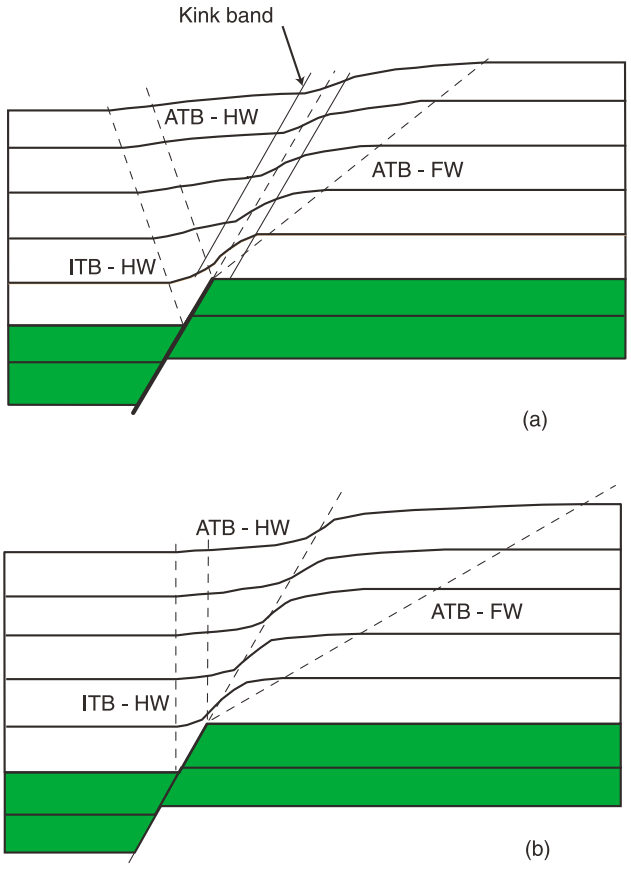

Fig. 2. Geometry predicted for extensional fault-propagation folds using Zehnder and Allmendinger's (2000) method. (a) Asymmetrical trishear model using piece-wise linear velocity field. $\phi_1 = 49°$ and $\phi_2 = 21°$. (b) Symmetrical trishear model using non-linear velocity field. The velocity field factor (r) = 3 and apical angle (ϕ) = 60°. ATB = active trishear boundary, ITB = inactive trishear boundary, HW = hanging wall, FW = footwall. The shaded layers are precut beds not involved in trishear deformation.

In this study, we propose a new general velocity field for the trishear model and a strain prediction method based on the specified velocity field. We first discuss the velocity distribution within the trishear zone in terms of a new parameter that governs the shape of the velocity field. Then we present numerical examples to show the importance of the trishear parameters in determining the final geometry of a structure. Finally, we apply the trishear model to predict the geometry and the strain distribution from experimentally deformed structures and a natural example from the Gulf of Suez shown in Fig. 1b. We demonstrate the advantages of the new model over the previous models and use strain to predict the orientation and distribution of fractures during progressive deformation following the approach of Zehnder and Allmendinger (2000).

2. The general velocity field model in a trishear zone

The basic assumptions for the kinematic trishear model discussed in this study are: (a) cross-sectional area is conserved throughout deformation; (b) the trishear zone may be symmetrical or asymmetrical with respect to the fault tip line; (c) the velocity in any area is continuous unless it is faulted. The velocity need not be linearly distributed throughout the trishear zone, nor need it be piecewise linear to achieve the asymmetry. In this paper, we employ an explicit way for deriving a new non-linear velocity field in a trishear zone, which is adapted from the approach of Zehnder and Allmendinger (2000).

Fig. 3 illustrates the basic geometry of the trishear model used for derivation of the general velocity field in the trishear zone. The fault is shown as horizontal for convenience. A triangular trishear zone lies at the tip of a fault with hanging wall apical angle ϕ_1 and footwall apical angle ϕ_2. The apical angle is $\phi = \phi_1 + \phi_2$. The velocity in the hanging wall is V_o, and the velocity in the footwall is 0, which means it is stationary. P is any point in the trishear zone whose velocity is to be calculated. QR is a line passing through P which is perpendicular to the fault plane. Q and R are intersecting points of the line with lower and upper boundaries of the trishear zone, respectively (Fig. 3).

The velocity field can be written in vector form as:

$$V(x, y) = V_x(x, y)\hat{i} + V_y(x, y)\hat{j}, \quad (1)$$

where x and y are parallel and perpendicular to the fault line and $\hat{i}$ and $\hat{j}$ are the unit vectors in the x, y directions. The line

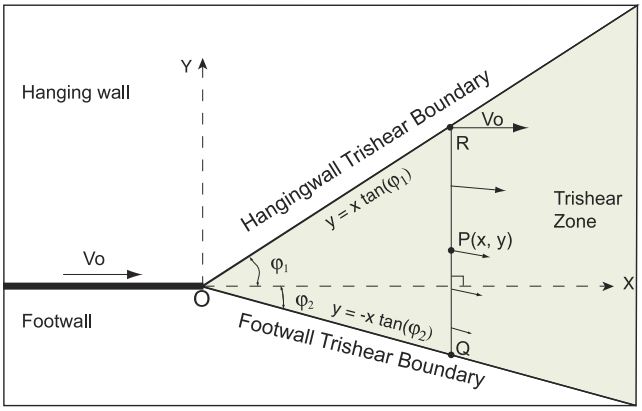

Fig. 3. Geometry of the trishear model and the coordinate system used in the text. The fault is shown as horizontal for convenience. Velocity in the hanging wall is V_o. It decreases nonlinearly from V_o at the boundary of trishear zone in the hanging wall to zero at the boundary in the footwall. ϕ_1 and ϕ_2, separated by the projected tip line of the fault, are the hanging wall and footwall apical angles of the trishear zone and are not necessarily the same. $P(x,y)$ is a referenced point whose velocity is to be calculated within the trishear zone.

QR is the direction along which Vx of the velocity field is varied in a certain way (linear, quadric, cubic, etc.).

The boundary conditions for the velocity field in the trishear zone are: velocity at the boundary between the trishear zone and the footwall is zero and the velocity is V_o at the boundary between trishear zone and hanging wall. That is:

$$\begin{aligned} &V_x = V_0, \quad V_y = 0, \quad \text{on } y = x\tan(\varphi_1), \\ &V_x = 0, \quad V_y = 0, \quad \text{on } y = -x\tan(\varphi_2) \end{aligned} \tag{2}$$

The condition that area is preserved is equivalent to the area being incompressible. In mathematical terms, the divergence of the velocity field is zero (Mase and Mase, 1992):

$$\mathrm{div}(V) = \frac{\partial V_x}{\partial x} + \frac{\partial V_y}{\partial y} = 0 \tag{3}$$

Assuming that the decrease of V_x of P is a function of the distance between PQ until it reaches point Q with zero velocity, and has the following form:

$$V_x = V_0\left(1 - \frac{L_{\mathrm{PR}}}{L_{\mathrm{QR}}}\right)^{1/r} = V_0\left(\frac{y - m_2 x}{(m_1 - m_2)x}\right)^{1/r} \tag{4}$$

where L_{PR} and L_{QR} are the distance between points PR and QR, respectively, $m_1 = \tan\phi_1$, $m_2 = -\tan\phi_2$, and r is a parameter that governs how V_x varies. The problem is therefore to find an explicit form of V_x in terms of V_0 and the location of point $P(x,y)$.

V_y can be solved by integrating V_x and Eq. (3).

$$\begin{aligned} \frac{\partial V_y}{\partial y} &= -\frac{\partial V_x}{\partial x} \\ &= V_0 \frac{y}{rx}\left(\frac{1}{(m_1 - m_2)x}\right)^{1/r}(y - m_2 x)^{((1/r)-1)} \end{aligned} \tag{5}$$

which yields

$$V_y = V_0\left(\frac{y + rm_2 x}{(r+1)x}\right)\left(\frac{y - m_2 x}{(m_1 - m_2)x}\right)^{1/r} + C \tag{6}$$

The constant C can be found by applying the boundary conditions (Eq. (2)). If a material point is located on the footwall trishear boundary where $y = m_2 x$, it is clear from Eq. (6) that

$$C = 0 \tag{7}$$

On the other hand, if a material point is located on the hanging wall trishear boundary where $y = m_1 x$, V_y also becomes 0. Apply this boundary condition to Eq. (6) to find

$$C = -\frac{m_1 + rm_2}{(r+1)} V_0 \tag{8}$$

From Eq. (7), it is clear that Eq. (8) becomes 0 as well for any material points located on the footwall trishear boundary. This yields the following important relationship:

$$m_1 = -rm_2 \tag{9}$$

Eq. (9) indicates that the velocity field in a trishear zone can be determined by measuring the hanging wall and footwall apical angles.

The final form of the velocity field in the trishear zone is given below:

$$V_x = V_0\left(\frac{y - m_2 x}{(m_1 - m_2)x}\right)^{1/r} \tag{10.1}$$

$$V_y = V_0\left(\frac{y + rm_2 x}{(r+1)x}\right)\left(\frac{y - m_2 x}{(m_1 - m_2)x}\right)^{1/r} \tag{10.2}$$

or in vector form:

$$\begin{aligned} V = {} & V_0\left(\frac{y - m_2 x}{(m_1 - m_2)x}\right)^{1/r}\vec{i} \\ & + V_0\left(\frac{y + rm_2 x}{(r+1)x}\right)\left(\frac{y - m_2 x}{(m_1 - m_2)x}\right)^{1/r}\vec{j} \end{aligned} \tag{11}$$

with the constraint of Eq. (9).

3. Strain in the trishear zone

Once the velocity field is specified, the strain or strain rate in the trishear zone can be determined from the velocity field. Suppose the strain is infinitesimal, where the initial referenced material points are displaced such that the squares and products of the displacement may be neglected

(Jaeger and Cook, 1979; Means, 1990). If the velocity field is specified by Eqs. (10.1), (10.2) or (11), then the strain rate, $\dot{e}$, in the x and y directions can be expressed as:

$$\begin{cases} \dot{e}_x = \dfrac{\partial V_x}{\partial x} = V_0 \dfrac{m}{r(m_1 - m_2)x} \left(\dfrac{m - m_2}{(m_1 - m_2)x} \right)^{((1/r)-1)} \\ \dot{e}_y = \dfrac{\partial V_y}{\partial y} = -V_0 \dfrac{m}{r(m_1 - m_2)x} \left(\dfrac{m - m_2}{(m_1 - m_2)x} \right)^{((1/r)-1)} \end{cases} \tag{12}$$

and the shear strain rate can be calculated as

$$\dot{\gamma}_{xy} = \frac{1}{2}\left(\frac{\partial V_x}{\partial y} + \frac{\partial V_y}{\partial x} \right) = \frac{V_0}{2r} \frac{(1 - m^2)}{(m_1 - m_2)x} \left(\frac{m - m_2}{(m_1 - m_2)} \right)^{((1/r)-1)} \tag{13}$$

where $m = \tan(y/x)$ The direction (θ) of the principal strain rate with respect to the x direction can be determined using (Jaeger and Cook, 1979):

$$\tan(2\theta) = \frac{2\dot{\gamma}_{xy}}{\dot{e}_x - \dot{e}_y} \tag{14}$$

For these directions, the elongation has maximum or minimum values that define the principal axes of strain or strain rate. The magnitudes of the principal strain rates are given by Jaeger and Cook (1979) as:

$$\dot{e}_{1,2} = \frac{1}{2}(\dot{e}_x - \dot{e}_y) \pm \left[\dot{\gamma}_{xy}^2 + \frac{1}{4}(\dot{e}_x - \dot{e}_y) \right]^{1/2} \tag{15}$$

where $\dot{e}_1$ and $\dot{e}_2$ represent the principal strain rates. The total principal strains are calculated as the summation of strain rates at each deformation step.

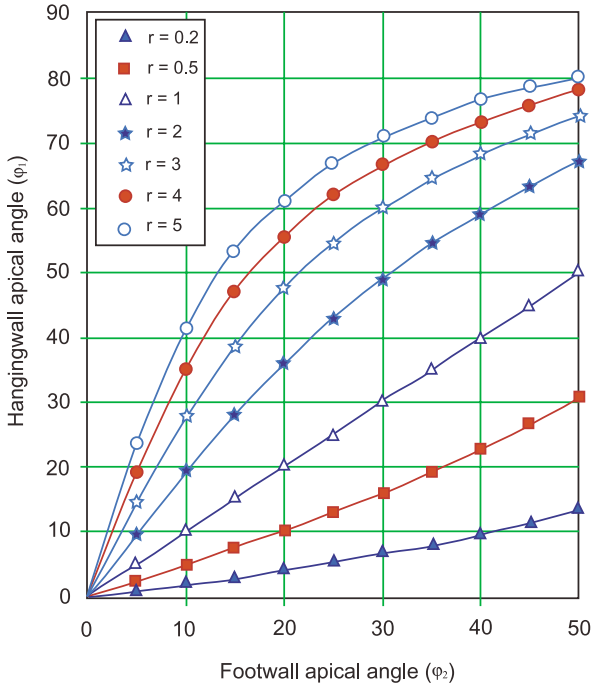

Fig. 4. The relationship between hanging wall and footwall apical angles and r in the trishear zone. If $r = 1$, the hanging wall and footwall apical angles are equal, which is the case of the linear velocity field described by Hardy and Ford (1997). When $r < 1$, the footwall apical angle is greater than the hanging wall apical angle while it becomes the opposite when $r > 1$. Note in the cases when r does not equal 1, a linear change of ϕ_1 does not result in a linear change of ϕ_2.

4. Implications of the shape factor r of the velocity field

The shape of the general velocity field described above is determined by the value of r and is depicted in Fig. 4. If $r = 1$, the linear velocity of Hardy and Ford (1997) is recovered. The constraint of Eq. (9), $\phi_1 = \phi_2$, indicates that the trishear zone has to be symmetrical with respect to the fault tip line. The velocity linearly decreases with respect to the distance from the hanging wall trishear boundary (Fig. 5).

The trishear zone is no longer symmetrical with respect to the fault tip line if $r \neq 1$. When $r > 1$, $m_1 > -m_2$, which results in $\phi_1 > \phi_2$ (Fig. 4). It is clear that more hanging wall material is involved in the deformation. In the hanging wall trishear domain, the velocity decreases very slowly. In the footwall domain, the velocity decreases rapidly (Fig. 5). This indicates that the strain rate is much higher in the footwall trishear domain than that in the hanging wall domain. When $r < 1$ and $\phi_1 < \phi_2$, the trishear zone is not symmetrical, and the velocity change and the associated strain rate are opposite to the case of $r > 1$. The quantitative relationship between r and the strain or strain rate will be discussed later.

Different combinations of values of ϕ_1, ϕ_2, and r define the nature of the deformation. If either ϕ_1 or ϕ_2 is close to zero, the other should also be close to zero if r is not too large. In this case, the trishear zone is very narrow, the hanging wall is deformed by rigid body translation and the footwall remains stationary. Thus, deformation by block faulting is simulated. When ϕ_1 is close to zero and r is very small, then ϕ_2 could be large enough (e.g. 20–30°) so that the trishear zone is extremely asymmetrical. With increasing displacement, an upward widening monocline will be produced that is confined to the footwall trishear zone. When ϕ_2 is close to zero and r is very large, then ϕ_1 could be large enough to produce an extremely asymmetrical trishear zone, with a monocline developed in the hanging wall. If $r = \infty$, the velocity within the trishear zone is constant and material in the trishear zone will move at the same rate as the hanging wall, which implies that the deformation tends to be brittle faulting.

Eq. (9) further reveals that r, ϕ_1 and ϕ_2 are not independent parameters specifying the velocity field. Only two of them are independent while the third is determined from the other two. The implication of this is that when dealing with a real deformed state cross-section, we can

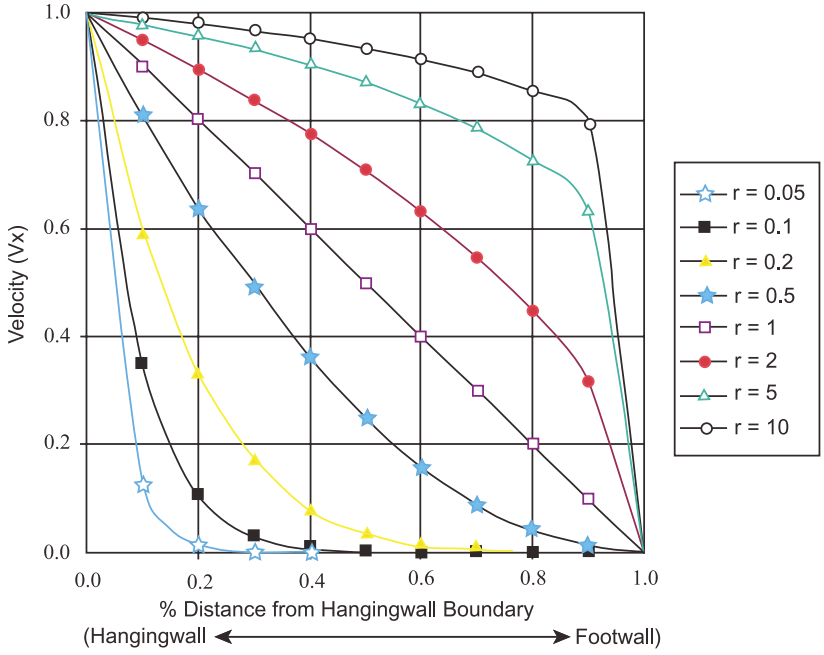

Fig. 5. The changes of velocity with relation to r in the trishear zone. When $r=1$, the velocity decreases linearly from the hanging wall to the footwall, which is the linear field discussed by Hardy and Ford (1997). When $r<1$, the velocity decreases rapidly in the hanging wall, indicating most displacement will occur in this region. When $r>1$, the decrease of velocity occurs mainly in the footwall.

measure ϕ_1 and ϕ_2 to determine the r value for either the forward modeling or restoration of the structure, which provides a practical and convenient way to specify the trishear parameters.

5. Influence of apical angle and *p/s* ratio

In order to discuss how the different apical angles and *p/s* ratios influence the final geometry of fault-propagation folds predicted by the general trishear model, we generate model runs with variable apical angles and *p/s* ratios. In each run, only one of those two parameters is changed, allowing the net effect of each parameter to be seen separately.

5.1. Variable apical angles

Fig. 6 shows the effect of different apical angles of the trishear zone on fold geometry. The apical angles used for generating the fault-propagation folds are 20, 40, and 60°. The fault does not propagate during deformation ($p/s=0$), and the fault tip is thus fixed to the footwall. Total slip along the fault is the same, and $r=0.8$ for all three cases.

The width of the fault-propagation fold is directly controlled by the apical angle of the trishear model (Fig. 6). With the increase of the apical angle, the deformation zone becomes wider and more open. With a small apical angle, bedding in the fault-propagation folds undergoes more rotation than bedding in folds with greater apical angles at the same stratigraphic level (Fig. 6a–c). Beds are thinned in the fold, with the most thinning occurring in the fault-propagation fold with smallest apical angle. More rotation of the fold limb and thinning of bedding are required to accommodate the deformation caused by displacement along the underlying fault as the width of the fold decreases.

5.2. Variable p/s ratio

Three fault-propagation folds with different *p/s* ratios are generated to investigate the direct influence of the *p/s* ratio (Fig. 7). The *p/s* ratio is the only parameter changed; all the other parameters are the same for all the fault-propagation folds. The apical angle is 60°, $r=0.8$, and the dip of fault is 60°. With increasing *p/s* ratio, the fault propagates upward faster and results in greater separation between the active trishear boundary and the inactive trishear boundary, which in turn results in less folding both in the hanging wall and the footwall (Fig. 7a–c). This is because once the fault cuts through the overlying beds, it stops the internal deformation in those beds and deformation becomes rigid-body translation. When the *p/s* ratio is large enough, the deformation is essentially rigid-body translation and there is no significant internal deformation within the trishear zone.

The *p/s* ratios also have great impact on the magnitudes of the strain in the trishear zone. The greatest strain is close to the fault tip in Fig. 7a for which the *p/s* ratio is zero. As the *p/s* ratio increases, beds have less time to deform before being cut by the fault and thus result in less strain. The strain ellipses within the area bounded by ITBs and ATBs in the model with a *p/s* ratio of 4.0 (Fig. 7c) are less flattened than

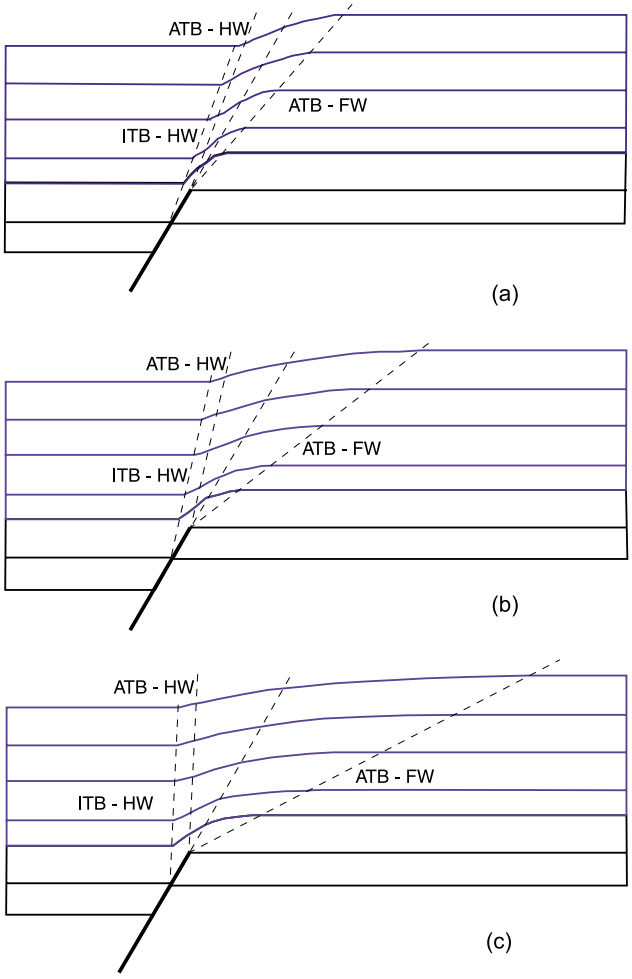

Fig. 6. Effect of different apical angles of the trishear zone on fold geometries. Apical angles are 20, 40, and 60° in (a), (b), and (c), respectively. In all three cases, the dip of fault is 60°, $r=0.8$, $p/s=0.0$, and the displacements along the faults are the same. ATB = active trishear boundary, ITB = inactive trishear boundary, HW = hanging wall, FW = footwall.

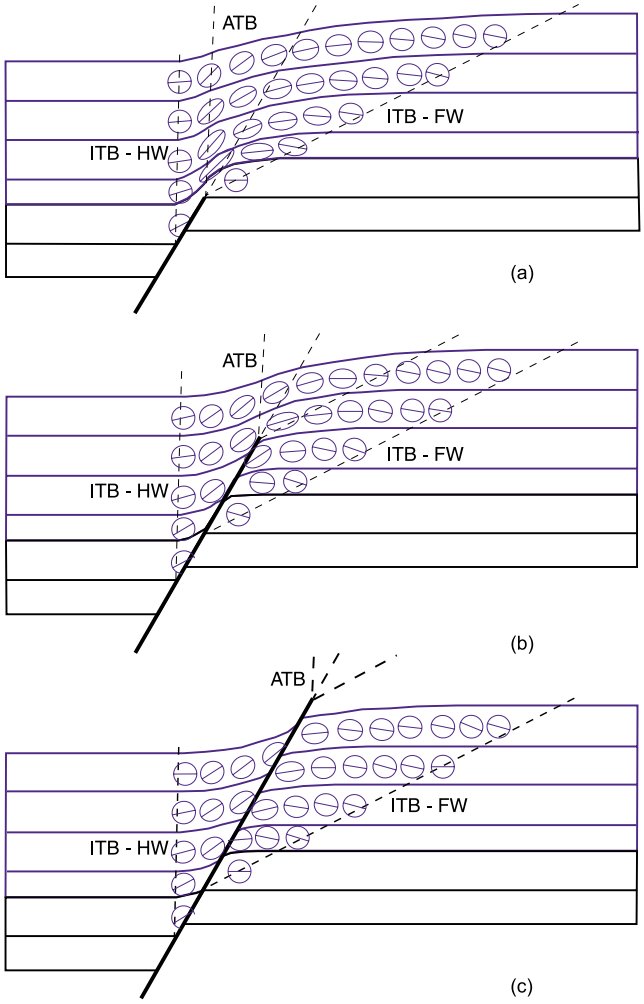

Fig. 7. The effects of different p/s ratios on the fold geometry and strain in the trishear zone. In all three cases, the fault dip = 60° and $r=0.8$. The p/s ratios are 0.0, 2.0, and 4.0 for (a), (b), and (c), respectively. The total slip along the faults is the same in all three cases. The line within the strain ellipses is the maximum extension direction. ATB = active trishear boundary, ITB = inactive trishear boundary, HW = hanging wall, FW = footwall.

those in the model with a p/s ratio of 0.0 (Fig. 7a and c). Less widespread secondary faulting or fracturing will be expected in deformation with greater p/s ratios.

6. Applications

In order to test how well the new trishear model predicts the geometry of extensional fault-propagation folds, we apply the technique to experimental folds developed above a 60° dipping normal fault and a vertical fault. We also apply this model to an extensional fault-propagation fold from the Gulf of Suez.

6.1. Experimental clay models

The experimental analog for a sedimentary sequence in the models is ball clay, which consists of approximately half clay-size quartz and half illite. The water content of the clay is adjusted until the first fault would appear at 10–15% strain in a pure shear experiment. On the side of the model, shallow horizontal grooves have been cut to provide bedding markers, and circles are marked to show strain. The basement consists of rigid wood blocks that can be displaced along a 60° normal fault (Fig. 8a) and a vertical fault (Fig. 8b). Models were photographed after every 0.5 cm of throw on the basement fault.

Experiment 09/14/78 (Fig. 9) is of a drape fold over a 60° dipping normal fault. The predicted geometry from the trishear model is superimposed on the images. The initial trishear boundaries (ITBs) for both the hanging wall and the footwall are determined from where the bed markers return to their regional elevations. The ϕ_1 and ϕ_2 measured from the ITBs are 32 and 38°, respectively (Fig. 9a), which defines $r=0.8$ and ϕ (total apical angle of the trishear

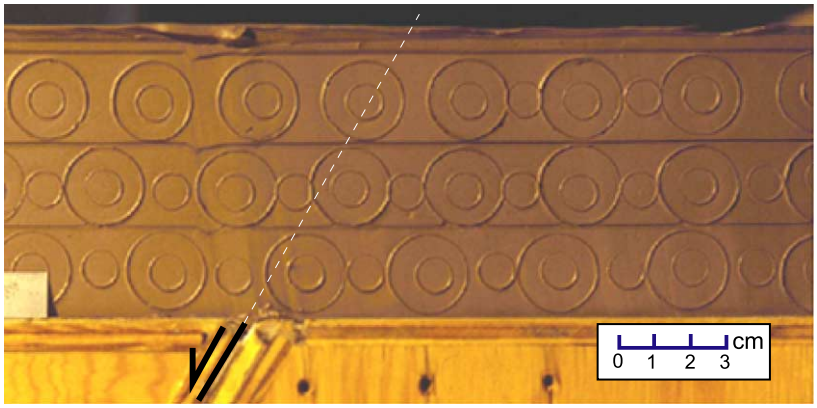

(a)

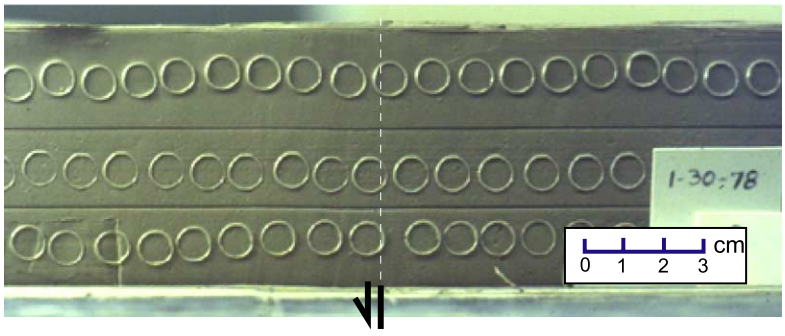

(b)

Fig. 8. Photos showing the pre-deformation stage of two experimental clay models in this study. Thin dashed lines are the extension of fault tip lines. Pre-cut faults are marked by thick black lines with arrows indicating the sense of movement. (a) Model 09/14/78, the basement fault dips 60° to the left. (b) Model 01/30/78, the fault is vertical.

zone) = 70°. Secondary faults with visible displacements began to develop after 1.0 cm of throw and are intensified in the final stage of the deformation where the throw is 2.0 cm. Since the model shows that the fault is propagating upward into the clay with a steeper dip in later stages of deformation, we use a *p*/*s* ratio of 4.0 to propagate the fault from 1.0 to 1.5 cm and 3.0 from 1.5 to 2.0 cm throw, respectively.

The predicted geometry for the fault-propagation fold matches well with the experimental model at all stages of displacement (Fig. 9). Many structural features of the analog model are accurately reproduced by the trishear model. In particular, the evolution of the monocline and the hanging wall syncline that develop adjacent to the fault are very similar to those predicted with the trishear model. The upward widening of the hanging wall fault-propagation fold is also reproduced. It can also be seen that the bed thickness in the trishear zone is less than outside the zone in both the analog model and the trishear model. The amount of thinning is not uniform throughout the trishear zone. The beds in the hanging wall trishear domain have experienced more thinning than those in the footwall domain. This is because the velocity field specified by the parameters suggests that the greater velocity gradient in the hanging wall results in more shear deformation in that domain than in the footwall domain. Because there is more area in the footwall involved in the deformation, the velocity gradient is fairly small and hence little reduction in bed thickness is produced.

The amount of strain and its distribution are also well predicted by the trishear model (Figs. 9 and 10). The strain ellipses in the hanging wall fault-propagation fold are more deformed than those in the footwall. This is the result of the greater velocity gradient in the hanging wall trishear domain. The orientation of the maximum principal stretch in Fig. 9 becomes progressively closer to parallel with the bedding in the monocline with the increase of the displacement. From the hanging wall trishear boundary to the footwall boundary, the orientation of the maximum elongation becomes progressively more oblique to bedding.

The orientations of minor faults are well predicted by the trishear model (Fig. 10). We used the criterion of Allmendinger (1998), that the orientations of the lines of no finite elongation (LNFE) in the strain ellipses predict the orientation of minor faults. The LNFEs in the kinematic model mimic remarkably well the observed minor fault

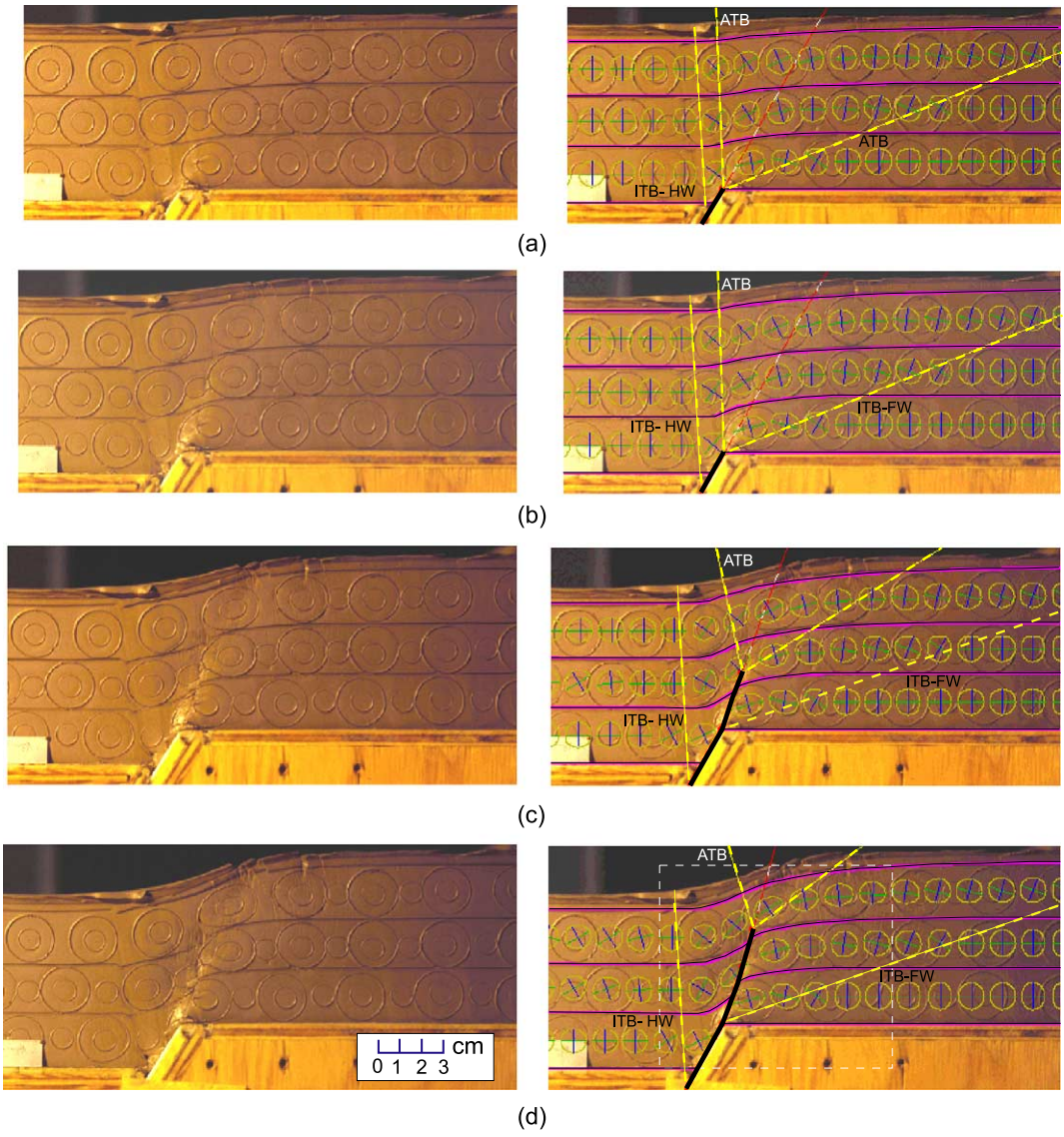

Fig. 9. Sequential deformation and trishear modeling of experiment 09/14/78. The uninterpreted images are shown on the left and the trishear models are superimposed on the right. The basement fault begins to propagate up section after 1.0 cm throw. Strain ellipses predicted by the trishear model are shown, with a light line and a dark line representing the principal directions of elongation and shortening, respectively. The throws are 0.5, 1.0, 1.5, and 2.0 cm for (a), (b), (c), and (d), respectively. The dashed rectangle in (d) is the area shown in Fig. 10. ATB = active trishear boundary, ITB = inactive trishear boundary, HW = hanging wall, FW = footwall.

patterns in the clay model. Note that the minor faults are well developed within the area enclosed by the contour line with axial ratio of 0.95 (Fig. 10b), which indicates approximately 10% shortening along the minimum principal strain axis. The results indicate that the orientations of LNFEs are good indicators of the orientation of minor faults.

Experiment 01/30/78 is of a drape fold formed by differential vertical movement of a basement fault (Fig. 11). The deformed geometry is highly asymmetrical with a hanging wall (down-thrown zone) apical angle of 28.2° and a footwall (up-thrown zone) apical angle of 41.8°. The modeling parameters for the trishear model are apical angle = 70°, $r = 0.6$, and $p/s = 0.0$ for 0.5 and 1.0 cm throws. Again, the experiment is modeled at 0.5 cm intervals of throw. The basement fault propagates upsection into the clay after 1.5 cm throw. The propagation of the fault is modeled by a p/s ratio of 3.0 between 1.5 and 2.0 cm throws. At 2.0 cm throw there is reverse faulting in the hanging wall close to the master fault, which might be an edge effect. The predicted geometry of an upward widening monocline fits well the structure in the clay model. Thinning of beds occurs mostly directly above the fault tip and along the extension of the fault tip line. The rotation of strain axes is much more dramatic in this model because the vertical fault introduces a greater downward component of displacement in the hanging wall domain.

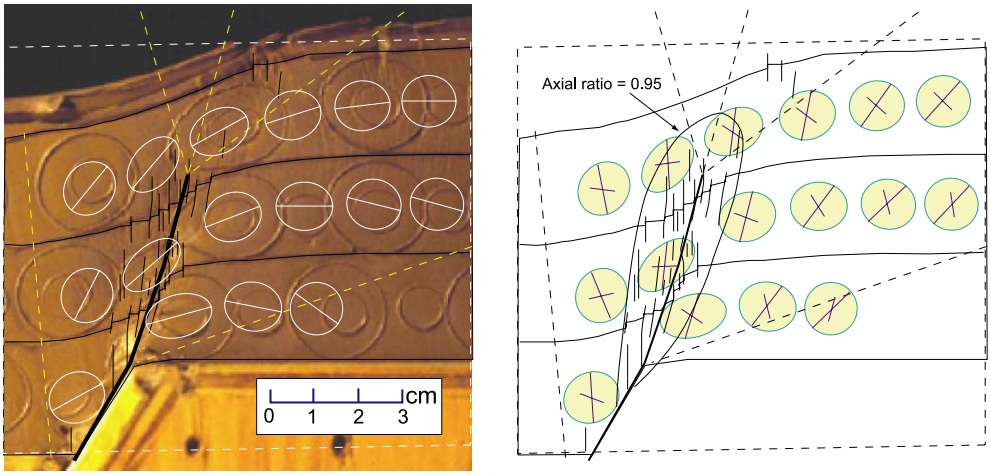

Fig. 10. Enlargement of final stage of normal fault experiment 09/14/78. Fault orientation is predicted using lines of no finite elongation (LNFEs) of strain ellipses calculated from the trishear velocity field. (a) Line drawings of small faults from the deformed clay model with the calculated strain ellipses superimposed on them. (b) LNFFs of strain ellipses and the faults copied from (a). Two sets of LNFEs are marked by a longer line and a shorter line in each ellipse. The orientation of longer lines of LNFEs matches those of faults from the clay model. The fractures are well developed within the area surrounded by the axial ratio 0.95 contour line indicated in (b).

6.2. The Gulf of Suez

The Gulf of Suez has long been recognized as having extensional fault-propagation folds formed by the upward propagation of basement faults (Robson, 1971; Garfunkel and Ronnevik, 1986; Withjack et al., 1990). Continental rifting began in the Suez area during the Oligocene and continues today. During rifting, steeply dipping normal faults formed within the Precambrian igneous–metamorphic basement, and extensional forced folds developed within the overlying Paleozoic through Cenozoic strata (Figs. 1b and 12). See Withjack et al. (1990), Garfunkel and Ronnevik (1986), and Coffield and Schamel (1989) for further details about the regional geological setting and structures of the area.

We apply the trishear technique to model the geometry of the cross-section (Fig. 12) from the Gulf of Suez reported by Withjack et al. (1990). The hanging wall and footwall apical angles are 27 and 23° as determined by measurement from the cross-section (Fig. 12). The value r for the velocity field is thus 1.2. Because the regionals from both the hanging wall and footwall in the original cross-section are tilted to the east, they are restored to horizontal for modeling purposes by rotating the cross-section about 5° counter-clockwise. The initial fault tip was located at the top of the basement, because the inactive trishear boundaries terminate at the fault cutoffs of the top basement. During the deformation, the basement fault is interpreted to have continuously propagated upsection with the same dip.

The general geometric features of the deformed structure in the cross-section are predicted by the trishear model (Fig. 12). The shape of bedding in the hanging wall syncline and the footwall anticline closely matched the predicted structure. The predicted structure for the Paleozoic and Cenozoic strata provides detailed information about the slip and the locations of stratigraphic boundaries, especially for those beds that were eroded away in the footwall. The trishear model successfully predicts the stratigraphic boundaries and dip of bedding at the level of exposure on the original cross-section where detailed outcrops are available for direct validation of the model. A very slight mismatch appears at the top of the Precambrian basement in the footwall. However, because the geometry of the strata at that level is poorly controlled by the data available (Withjack et al., 1990), this does not invalidate the applicability of the trishear model.

An important feature in Fig. 12 is that the beds in the hanging wall do not dip progressively steeper from the younger units to the older ones. From experimental models and our previous discussion on the trishear models, progressive downward steepening of beds results from an underlying fault that does not propagate or that propagates at a constant rate. To prevent a downward increase in dip, two different p/s ratios must be used in trishear modeling. The fault propagates at a p/s ratio of 2.0 in the Paleozoic/Upper Cretaceous Nubia sandstone (PKn) followed by a reduced p/s ratio of 1.2 as the fault propagates across the higher formations that consist of interbedded clastics and carbonates. This could be explained if the sandstone is more brittle, and the interbedded limestone and shale can more readily fold, hence the fault propagates faster in the sandstones than it does in the mixed layered sequence.

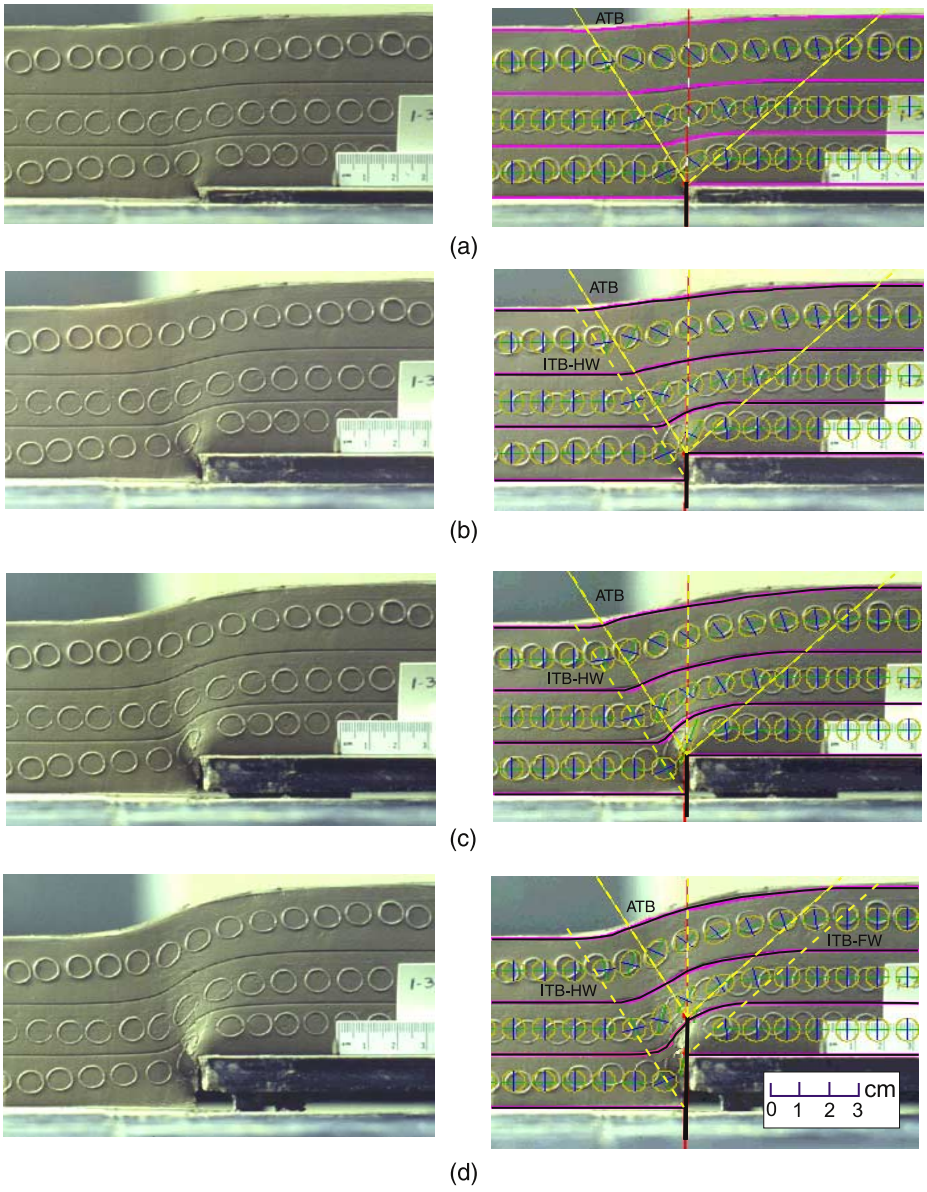

Fig. 11. Sequential deformation and trishear modeling of vertical fault experiment 01/30/78. The uninterpreted images are shown on the left and the trishear models superimposed on the right. The basement fault begins to propagate after 1.5 cm of throw. Strain ellipses predicted by the trishear model are shown. Throws are 0.5, 1.0, 1.5, and 2.0 cm for (a), (b), (c), and (d), respectively. ATB = active trishear boundary, ITB = inactive trishear boundary, HW = hanging wall, FW = footwall.

7. Discussion

The non-linear trishear model proposed in this paper is superior to the linear model in predicting the geometry of trishear structures with high bedding curvature. The shape factor (r) of the velocity field dictates the bedding curvature. To illustrate this, the folds predicted using a linear velocity field identical to Hardy and Ford's (1997) model are applied to the previous experimental models in Fig. 13. The apical angles and p/s ratios are the same as those in our model. It can be seen that the linear velocity model predicts the trishear geometry fairly well for the drape over the normal fault, whereas there are significant mismatches in the drape over the vertical fault. The mismatch is best described by the difference between the high bedding curvature in the clay model and the lower bedding curvature from the linear trishear model. The linear velocity field produces a relatively low velocity gradient from the hanging wall trishear domain to the footwall domain which in turn results in a lower predicted bedding curvature than does the non-linear field ($r = 0.6$, Fig. 11).

Generally, smaller values of r produce smoother and greater curvatures. When r is small, velocity decreases rapidly in the hanging wall and thus creates a large velocity gradient. In the footwall, both the velocity and its gradient are much smaller. Therefore, the displacement caused by

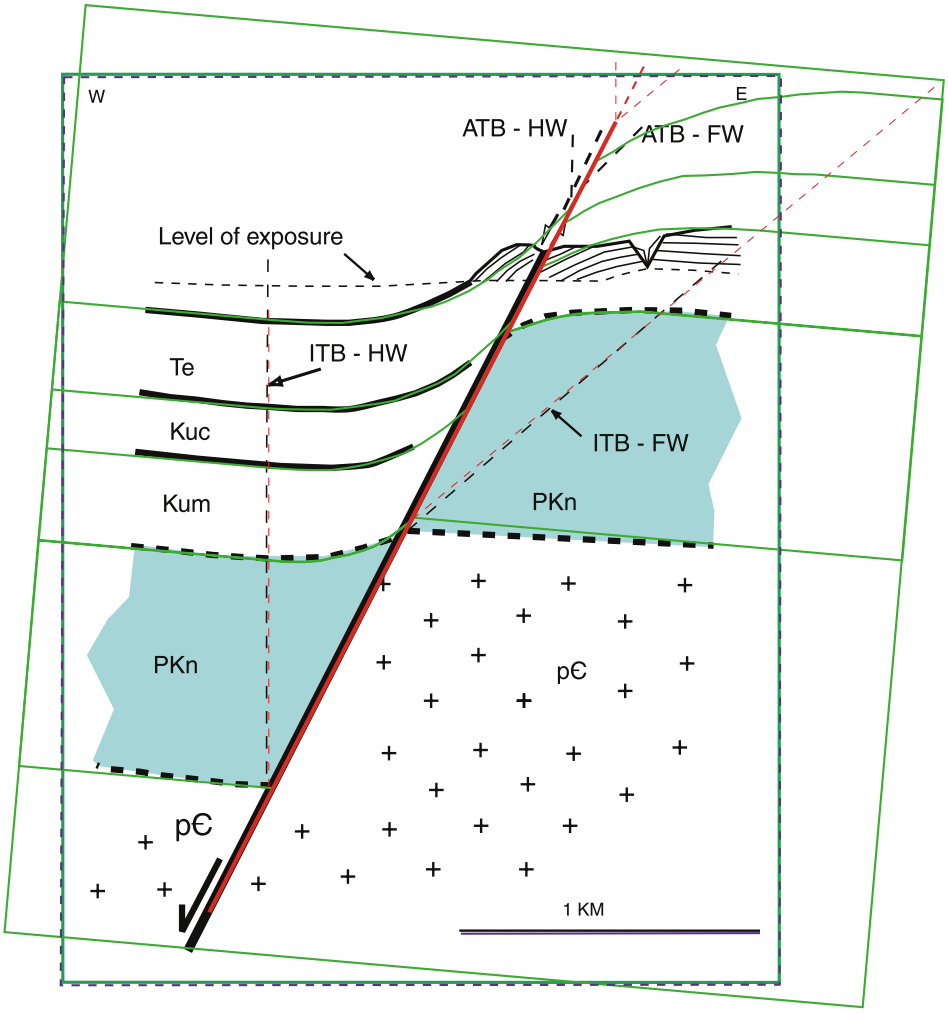

Fig. 12. Trishear predicted geometry and strain of an extensional fault-propagation fold from the Gulf of Suez based on the cross-section from Withjack et al. (1990). Before modeling, the regionals in both the hanging wall and footwall are restored to horizontal by rotating the original cross section 5°. The modeling parameters are measured from the deformed cross-section as: hanging wall apical angle = 27°, footwall apical angle = 23° and the resulting $r = 1.2$. The fault propagates upsection with $p/s = 2.0$ in the Pkn formation and $p/s = 1.2$ in the younger units. See Fig. 1 for explanation of original cross-section.

fault slip is mainly accommodated by folding in the hanging wall. The highest curvature is usually present in the hanging wall accompanying the greatest thinning of bedding in extensional settings. A much wider zone is involved in deformation in the footwall, and this deformation is characterized by small bedding curvature and slight bedding thinning. If a geological structure is reproduced by a trishear model with a small velocity shape factor (say, $r = 0.5$), it probably indicates that the ductility of the rock involved in the deformation is high and less secondary faulting will be present.

The relationship between the hanging wall apical angle, the footwall apical angle, and r in the trishear model provides a convenient and approximate estimation of the velocity field in the forward modeling of natural and experimental structures. One of the problems associated with the previous trishear models is the fact that the values of the modeling parameters are hard to determine before applying them to a real structure. The modeling has to be accomplished by a trial-and-error method to determine the final parameters. By using the relationship discussed in this paper, one can easily measure the hanging wall and footwall apical angles from a deformed structure and the velocity field in a trishear zone is automatically determined. One can therefore use these initial values for the trishear parameters to model the actual structures without the need for generating a broad array of possible values.

The directions of secondary faults can be predicted from the strain ellipses calculated from the trishear model. Because the strain of rocks can be accommodated in a variety of ways, no individual strain indicators will necessarily match the strain ellipses predicted with the trishear forward models. The most reliable measure of strain in the structure is the change in bedding thickness itself (Allmendinger, 1998). If a trishear forward model matches the thickness changes throughout a real structure, then the

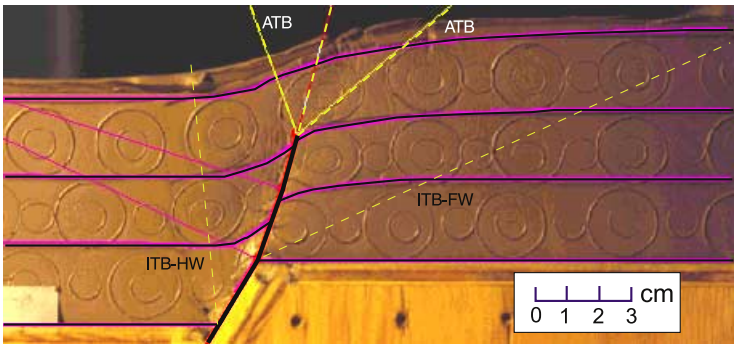

(a)

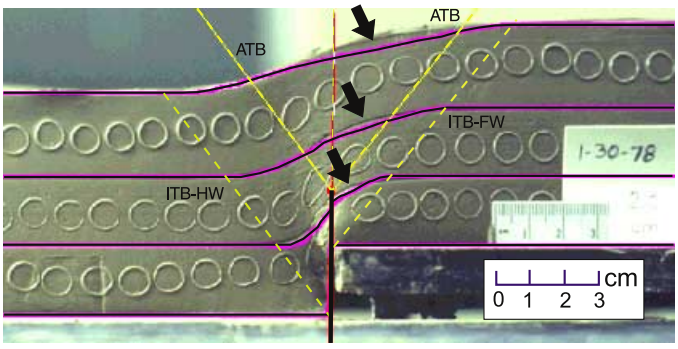

(b)

Fig. 13. Trishear predictions of experimental models using Hardy and Ford's (1997) linear velocity field. (a) Experiment 09/14/78, apical angle = 70°. (b) Experiment 01/30/78, apical angle = 75°. Fault throw is 2.0 cm for each model. Thin black lines are predicted bedding, thin white lines are predicted trishear boundaries. Arrows indicate the locations of greatest bedding mismatch.

predicted strain must be consistent with the bulk strain in the real structure. Allmendinger (1998) and Watterson (1999) suggested that failure along zero extension directions rather than stress ellipses can be applied to natural structures in rocks. The zero extension directions are identical to the direction of LNFEs of strain ellipses. The orientation and population of secondary faults in the models can be predicted by strain ellipses using LNFEs with reasonable confidence.

8. Conclusions

The trishear model is a powerful and useful tool for modeling extensional fault-propagation structures. It can produce a wide range of fault-related, upward-widening structures that are commonly observed in extensional settings. The velocity field within a trishear zone derived in this paper can be used to model asymmetrical fault-propagation folds, which makes it more applicable to real structures than previous models. The shape factor of the velocity field dictates how the velocity decreases from the hanging wall to the footwall and hence controls the curvature and smoothness of the deformed bedding structure. The strength of the new trishear model proposed here is that the velocity field can be easily specified by measuring the hanging wall and footwall apical angles and thus one can immediately begin the process of modeling a real structure.

The *p*/*s* ratio has a significant impact on the geometry of bedding and the strain within trishear folds. A greater *p*/*s* ratio results in faster upward fault propagation and hence produces narrower and less deformed fault-propagation folds. Beds will stop shearing and rotation and will be displaced by rigid body translation if a fault cuts through them during upward propagation. Typically, the strain of beds within a trishear zone becomes smaller as the *p*/*s* ratio increases.

The strain prediction model based on the trishear velocity field provides an explicit estimation of the magnitude and orientation of the strain ellipses throughout a trishear zone. The lines of no finite elongation of the strain distribution are good predictors of the orientations of second-order faults as proposed by Allmendinger (1998).

Acknowledgements

The Department of Energy Grant (Contract DE-AC22-94PC91008 through BDM-Oklahoma, Incorporated subcontract G4S51733) provided partial support of this research. Special thanks go to A. Zehnder and R. Allmendinger for a preprint of their manuscript on numerical trishear modeling. Thanks to Jack Pashin, Dennis Harry, and Charles Haynes for their helpful reviews. We thank Gloria Eisenstadt and Eric Erslev for their constructive reviews of the manuscript. This paper represents a portion of the senior author's PhD dissertation at the University of Alabama.

References

Allmendinger, R.W., 1998. Inverse and forward numerical modeling of trishear fault-propagation folds. Tectonics 17, 640–656.

Coffield, D.Q., Schamel, S., 1989. Surface expression of an accommodation zone within the Gulf of Suez, Egypt. Geology 17, 76–79.

Erslev, E.A., 1991. Trishear fault-propagation folding. Geology 19, 617–620.

Erslev, E.A., Rogers, J.L., 1993. Basement-cover geometry of Laramide fault-propagation folds. In: Schmidt, C.J., Chase, R.B., Erslev, E.A. (Eds.), Laramide Basement Deformation in the Rocky Mountain Foreland of the Western United States: Special Paper. Geological Society of America, Boulder, CO, pp. 125–146.

Ferrill, D.A., Morris, A.P., Sims, D.W., Waiting, D.J., Hasegawa, S., 2004. Development of synthetic layer dip adjacent to normal faults. In: Sorkhabi, R., Tsuji, Y. (Eds.), Faults, Fluid Flow, and Petroleum Traps American Association of Petroleum Geologists Memoir. American Association of Petroleum Geologists, Tulsa, OK, USA, pp. 125–138.

Garfunkel, Z., Ronnevik, H., 1986. Tectonics of the Suez rift. Bulletin of the Geological Survey of Israel 71, 1–44.

Gawthorpe, R.L., Sharp, L., Underhill, J.R., Gupta, S., 1997. Linked sequence stratigraphic and structural evolution of propagating normal faults. Geology 25, 795–798.

Hardy, S., Ford, M., 1997. Numerical modeling of trishear fault-propagation folding and associated growth strata. Tectonics 16, 841–854.

Hardy, S., McClay, K., 1999. Kinematic modeling of extensional fault-propagation folding. Journal of Structural Geology 21, 695–702.

Jaeger, J.C., Cook, N.G.W., 1979. Fundamentals of Rock Mechanics. Chapman & Hall, London. 593pp.

Janecke, S.U., Vandenburg, C.J., Blankenau, J.J., 1998. Geometry, mechanisms, and significance of extensional folds from examples in the Rocky Mountain Basin and Range province, USA. Journal of Structural Geology 20, 841–856.

Jin, G., Pashin, J.C., Groshong, Jr. R.H., 1998. Well-based 3-D visualization of mature oil reservoirs associated with the Gilbertown graben, southwest Alabama. AAPG 1998 Annual Convention, Salt Lake City.

Laubscher, H.P., 1982. Die Sudosttecke des Rheingraben—ein kinematisches und dynamisches problems. Eclogae Geologicae Helvetiae 75, 101–116.

Mase, G.E., Mase, G.T., 1992. Continuum Mechanics for Engineers. CRC Press, Boca Raton, FL.

Means, W.D., 1990. Kinematics, stress, deformation, and material behavior. Journal of Structural Geology 12, 953–971.

Pashin, J.C., Raymond, D.E., Alabi, G.G., Groshong Jr., R.H., Jin, G., 2000. Revitalizing Gilbertown oil field: characterization of fractured chalk and glauconitic sandstone reservoirs in an extensional fault system. Geological Survey of Alabama Bulletin 168, 1–81.

Patton, T.L., Fletcher, R.C., 1995. Mathematical block-motion model for deformation of a layer above a buried fault of arbitrary dip and sense of slip. Journal of Structural Geology 17, 1455–1472.

Robson, D.A., 1971. The structure of the Gulf of Suez (Clysmic) rift, with special reference to the eastern side. Journal of the Geological Society 127, 247–276.

Schlishe, R.W., 1995. Geometry and origin of fault-related folds in extensional settings. American Association of Petroleum Geologists Bulletin 79, 1661–1678.

Watterson, J., 1999. The future of failure: stress or strain. Journal of Structural Geology 21, 939–948.

Withjack, M.O., Meisling, K.E., Russell, L.R., 1989. Forced folding and basement-detached normal faulting in the Haltenbanken area, offshore Normay. In: Tankard, A.J., Balkwill, H.R. (Eds.), Extensional Tectonics and Stratigraphy of the North Atlantic Margins AAPG Memoir 46, pp. 567–575.

Withjack, M.O., Olson, J., Peterson, E., 1990. Experimental models of extensional forced folds. American Association of Petroleum Geologists Bulletin 74, 1038–1054.

Zehnder, A.T., Allmendinger, R.W., 2000. Velocity field for the trishear model. Journal of Structural Geology 22, 1009–1014.